INTERNATIONAL JOURNAL OF HYDROGEN ENERGY 48 (2023) 1146–1159

Available online at www.sciencedirect.com

ScienceDirect

journal homepage: www.elsevier.com/locate/he

Evolution and distribution of the anode overpotential and its oscillations in a polymer electrolyte membrane fuel cell exposed to carbon monoxide

Velia F. Valdés-López [a,*], *Luis Castanheira* [b], *Gareth Hinds* [b], *Thomas Bacquart* [b], *J.I.S. Cho* [a], *Tom Mason* [a], *Paul R. Shearing* [a], *Daniel J.L. Brett* [a]

[a] *Electrochemical Innovation Lab, University College London, Torrington Place, London, WC1E 7JE, United Kingdom*
[b] *National Physical Laboratory, Teddington, Middlesex, TW11 0LW, United Kingdom*

HIGHLIGHTS

- In situ measurements of anode overpotential performed in the presence of CO.
- Local operating conditions had an impact on distribution of adsorbed CO.
- Spatiotemporal dynamics observed, including self-sustained potential oscillations.
- Coexistence of dominant mean-field and migration coupling areas identified.

ARTICLE INFO

Article history:
Received 27 July 2022
Received in revised form
23 September 2022
Accepted 2 October 2022
Available online 25 October 2022

Keywords:
Polymer electrolyte membrane fuel cell
CO poisoning distribution
Self-sustained potential oscillations
Anode overpotential
Localised reference electrode
Mean-field and migration coupling

ABSTRACT

Carbon monoxide (CO) poisoning of polymer electrolyte membrane fuel cells (PEMFCs) remains a challenge for their deployment, and a deeper understanding of the spatiotemporal dynamics involved is needed to develop effective mitigation strategies. In this work, localised reference electrodes were used to measure the anode overpotential at three locations across the active area of a galvanostatically operated cell (0.3 A cm^{-2}) exposed to 100 ppm CO/H_2. The anode region closest to the inlet was poisoned more rapidly than the rest of the cell, following a sigmoidal variation, and presented a higher CO coverage. The varying CO concentration, combined with local operating conditions, had a direct impact on the distribution of CO coverage. Additionally, complex self-sustained oscillations of the cell voltage and the anode overpotential were observed and correlated with the rate of CO oxidation in the overall cell. The coexistence of a dominant mean-field coupling area closer to the anode inlet, and a dominant migration coupling region closer to the outlet was identified, consistent with reported modelling predictions for a single straight channel cell. Finally, the cell recovery with pure H_2 was shown to be a faster process than the CO adsorption, which follows first-order kinetics and is affected by local conditions.

© 2022 The Authors. Published by Elsevier Ltd on behalf of Hydrogen Energy Publications LLC. This is an open access article under the CC BY license (http://creativecommons.org/licenses/by/4.0/).

* *Corresponding author.*
E-mail address: fabiola.valdes.13@ucl.ac.uk (V.F. Valdés-López).

https://doi.org/10.1016/j.ijhydene.2022.10.007

0360-3199/© 2022 The Authors. Published by Elsevier Ltd on behalf of Hydrogen Energy Publications LLC. This is an open access article under the CC BY license (http://creativecommons.org/licenses/by/4.0/).

Introduction

Polymer electrolyte membrane fuel cells (PEMFCs) are a promising electrochemical energy conversion technology that can help transition from fossil fuel dependence and reduce carbon dioxide emissions. They have received much attention for a wide range of applications [1]. However, the availability of a hydrogen fuelling infrastructure is a barrier to their uptake, and the quality (purity) of that hydrogen has a significant impact on the extent of performance degradation. As the majority of hydrogen is currently generated through steam reforming of natural gas, carbon monoxide (CO) is present to varying degrees, depending on the level of post-processing performed to purify the hydrogen [2]. CO is usually introduced by the hydrogen fuel supply and competes with hydrogen for the active sites on the platinum of the anode electrocatalyst. CO adsorbs on the catalyst surface, reducing the available surface for the hydrogen oxidation reaction (HOR). Just trace (ppm) amounts of CO have a pernicious effect on the performance of PEMFCs operating at typical temperatures of 80 °C [3].

The dynamics of CO adsorption and the effect on performance are complex and often result in the voltage of cells oscillating when operated under galvanostatic control [4–6]. Electrode potential oscillations under constant current were first reported in 1969 [7]. As the CO accumulates on the surface of the catalyst, the anode overpotential increases until a threshold is reached where CO oxidation occurs (to CO_2), removing it from the surface and reversing the poisoning effect. As the anode potential decreases (reduced overpotential), the CO is once again able to adsorb, the electrode is poisoned and the anode overpotential increases. The process is repeated, leading to anode overpotential oscillations. These oscillations were first reported for Pt–Ru/C catalysts [5,6], followed by Pd–Pt/C, Pd/C [8,9] and Pt/C [10]. Single-cell studies on CO poisoning have revealed the effect of different parameters on the frequency of the oscillations. As a general rule, the period decreases with an increase of the CO concentration or the anode flow rate. The period is also shorter with increasing current density or temperature [5,11]. Other studies have focused on the patterns of the oscillations. Mota et al. observed periodic and non-periodic states at different conditions of flow and current density. The transition from a period with one to two maxima peaks and chaotic states occurs with increasing current density at a fixed anode flow rate, or with decreasing flow rate at constant current [12].

The measurement of current and voltage across a range of electrical loads (the polarisation curve) is the most commonly used means of assessing fuel cell performance. While it represents the ultimate output of a cell or stack, a crude bulk measurement withholds the complexity of what is occurring across the active area of the electrodes. In fact, there will be a distribution of performance such that local current density, temperature, water composition and reaction conditions vary across the electrodes in both space and time. Localised measurement of these parameters is now extensively performed [13–17] and such measurements have been responsible for many new insights that have led to advanced hardware design and operating protocols. This work aims to uncover new information about the nature of CO poisoning by taking account of the spatial variations and temporal dynamics that occur during CO poisoning; in particular, the spatially varying characteristics that accompany potential oscillations. This is achieved using an array of reference electrodes (REs) to probe the local electrode potential. In addition, measurement of the CO_2 concentration in the exit gas is used to corroborate the existence of the oscillatory mode as being linked to CO oxidation.

Bulk voltage measurements of cells poisoned with CO have shown that the process is a function of many factors, including temperature [18], water content/gas humidification [19–22], CO concentration [3], anode gas flow rate [23], pressure [24], etc. Taking this into account and adopting a local view (individual location on an electrode) of fuel cell operation, it is clear that the process of CO poisoning is highly complex, as each of these factors will vary across the active area of a cell. What is more, local variations in one parameter can affect the situation elsewhere in the cell. For example, in the absence of self-sustained oscillations (typically low concentrations of CO), an uneven current distribution is observed under galvanostatic control as a result of the more rapid adsorption of CO at the inlet compared to the outlet [25–30]. Moreover, a pseudo-inductive behaviour at low frequencies has also been observed in the first segments (anode entrance) of cells using segmented electrochemical impedance spectroscopy (EIS) [25,26]. A more complex response is therefore anticipated in the local electrode potential measurements under oscillatory behaviour.

Experimentally observed patterns of operation have been explained by spatiotemporal models that proposed the visualisation of the system as a series of individual oscillators with additional interactions, including CO oxidation throughout the channel and two main interactions occurring between them: mean-field (global) coupling and migration (local) coupling [31,32]. The pattern observed depends on the dominant interaction. A change of state in a globally coupled system at a specific location is felt equally in the rest of system. A recognized globally coupled system is CO oxidation at Pt single-crystal surfaces [33–35]. A dominant mean-field coupling in a PEMFC exposed to CO under galvanostatic control, combined with a high reactant (H_2/CO) flow rate results in a homogeneous distribution of CO on the electrode surface and oscillations that are in phase and present a well-defined shape and single frequency. A reduction in the flow rate leads to more heterogeneous distribution of CO poisoning across the electrode surface [36] and results in more complex oscillatory behaviour, typically marked by period-doubling bifurcation of the homogeneous oscillation. Period-doubling bifurcation is a route to chaos, where the oscillations do not continue regularly and the periods between oscillations continually double, typically denoted as 'period-*n*'. In the case of dominant migration coupling, the interaction acts purely locally given a large and thin electrolyte, and is related to the appearance of electrochemical turbulence (spatiotemporal chaos), reflected by phase or defect turbulence. Small disturbances in the phase relation between adjacent oscillators are characteristic of the phase turbulence, while local aperiodic breakdowns of the oscillation amplitude, so-called phase slips, are specific to the defect turbulence. These two types of

chaotic behaviour are typical of the Benjamin-Feir instability that can be applied to the mechanisms involved in the transition from homogeneous to heterogeneous spatio-temporal states in reaction-diffusion systems [37–39]. Limited experimental studies have demonstrated the appearance of electrochemical turbulence, although Kirsch et al. validated its occurrence in a PEMFC exposed to CO under potentiostatic control in a six-straight-channel cell [40]. Mean-field and migration coupling have been observed experimentally in the oxidation of CO on Pt-based electrocatalysts; however, their appearance has not been evaluated under more realistic operating conditions in fuel cells.

This study aims to explore how cells enter the oscillation mode from a localised perspective and answer questions like: is the active area of the cell poisoned evenly and at the same rate? Do the oscillations start in one region and extend to the entire cell? Do different parts of a cell oscillate at different frequencies, with different amplitude or phase? Do rational trends exist across the active area of a cell? Are the existing models useful to understand the mechanisms occurring throughout a standard cell? These issues are important for developing mitigation strategies for CO poisoning [41], improving performance by spatially distributing catalyst type and composition across electrodes and understanding if and how one cell oscillating can affect other cells in a stack.

Experimental

A 50 cm^2 electrode area, in-house fabricated single-cell PEMFC with a six-channel partial counter-flow serpentine geometry was used. The MEA was composed of two identical Pt/C electrodes (Johnson Matthey), 0.4 mg cm^{-2} Pt loading, and a membrane electrolyte (Nafion HP, 22 μm thickness). The cell assembly was hydraulically compressed at 7 barg, and the variation and distribution of the anode potential was monitored through an array of three localised reference electrodes (REs), numbered following the hydrogen path. The localised REs allowed the direct measurement of the anode potential during the CO poisoning, isolating it from other components that have been proven to be affected by CO to a lower degree, such as the membrane [42] and the cathode [43,44]. Previous work calculated the anode [5] and overall [25,45] overpotential changes from cell voltage measurements using pure H_2 and a CO/H_2 mixture. Moreover, the localised RE configuration is not limited by the ohmic drop, potential distribution and electrode edge effects that conventional reference electrodes sustain in fuel cells [46]. The structure and location of the REs is shown in Fig. 1.

The localised REs used were previously developed by Hinds et al. [46]. These involve the use of salt bridges composed of Nafion tubing inserted in a polytetrafluoroethylene (PTFE) sheath, filled with a solution of 0.5 M H_2SO_4. The Nafion tubing had an inner diameter of 0.64 mm and an outer diameter of 0.84 mm, while the PTFE sheath had an inner diameter of 1.01 mm and an outer diameter of 1.27 mm. Holes were drilled in the end-plate and the flow-field to allow direct contact of the salt bridges for each RE to different locations on the back of the gas diffusion layer (GDL). To allow for an ionic connection to the electrode, the GDL was impregnated with Nafion using a solution previously heated at 70 °C, composed of 50:50 by volume of a 10% dispersion of Nafion in water (Sigma Aldrich) and 2,2,3,3-tetrafluoro-1-propanol (Sigma Aldrich). O-ring seals were used to prevent any gas leakage from the flow-field. On the other end of the salt bridges, glass chambers containing Gaskatel GmbH hydrogen REs were located. Each one of these electrodes was previously calibrated using a saturated calomel electrode. The measurement and data acquisition of the local anode potentials were made every second through a NI-9205 32-channel analogue input module in a compact DAQ chassis (National Instruments, USA), controlled by a LabVIEW program.

The cell was operated using a commercial fuel cell test station (G50, Greenlight Power Technologies Inc.) The current was maintained during the experiment at a current density of 0.3 A cm^{-2} and the temperature of the cell was maintained at 70 °C using cartridge heaters inserted in the end-plates of the cell. Humidified streams of pure H_2 and air were introduced to the anode and cathode, respectively, at a stoichiometry of 2 on both electrodes. The pressure at the anode inlet was 1.25 kPag. These operating conditions are representative of real-world PEMFC operation and correspond to an overall cell voltage of ~0.7 V. A second G50 unit was used to heat the humidified CO/H_2 mixture, and the alternation with the pure H_2 stream was carried out through a three-way valve. The concentration of CO_2 in the exit gas was monitored over time using an infrared CO_2 detector (GMP343 from Vaisala), which was located in the anode outlet. Prior to the detector, a filter comprising a PTFE membrane of 1.2 μm porosity was connected in the anode outlet, followed by two cooling traps to remove water vapour from the stream.

The main experiment consisted of three phases: (i) an initial period of 30 min where the cell was operated with high purity H_2 (>99.99%), (ii) operation with a mixture of 100 ppm CO/H_2 for ~16 h, and (iii) a 1 h recovery stage with pure H_2. A CO concentration in H_2 of 100 ppm was chosen, as previous studies that considered Pt as catalyst had reported such oscillatory behaviour with this fuel composition and a similar operating temperature [10]. A relatively long exposure period to CO under oscillatory behaviour was considered as prior reports show oscillations during the space of minutes and even seconds [5,11,12,40,47–49], while long-term experiments were accomplished at lower CO concentration (<50 ppm CO/H_2) where no potential oscillations were observed [25,26,45,50–53]. In addition, preliminary experiments were carried out at two different CO concentrations (20 ppm and 50 ppm CO/H_2) and a current density of 0.5 A cm^{-2} in order to validate the experimental setup.

Results and discussion

The results obtained through the localised REs are presented according to the progression of the system, where different phases are identified: transition phase, two successive pseudo-steady states and recovery phase. Fig. 2 (a) presents the evolution of the cell voltage and the change in the anode overpotential due to CO, $\Delta\eta$, measured against each of the three reference electrodes, RE1, RE2 and RE3, during these

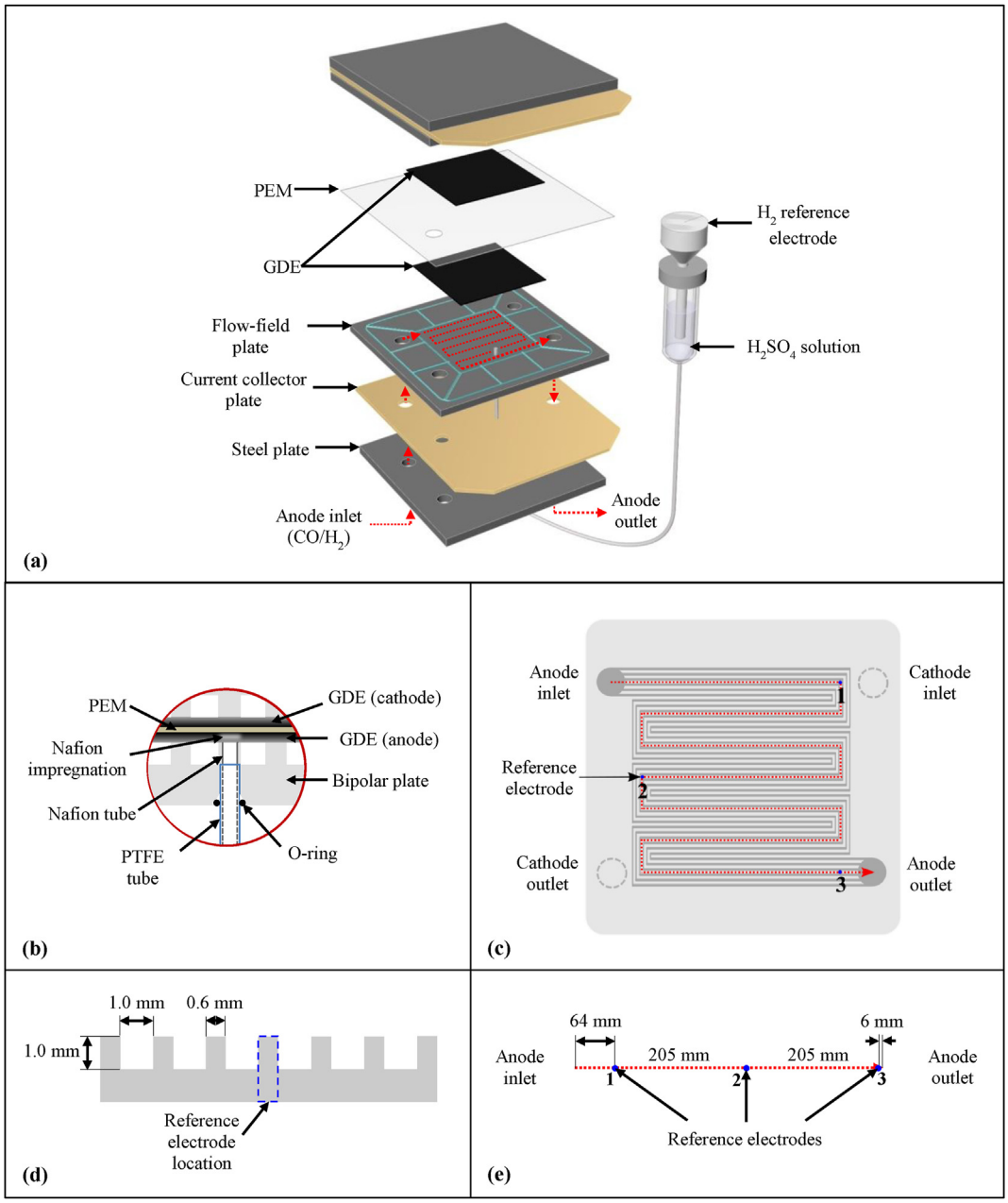

Fig. 1 – Placement of the REs in the 50 cm^2 PEMFC with a six-channel partial counter-flow serpentine geometry: (a) Configuration of the system in the presence of one RE; (b) insertion of the RE into the MEA; (c) location of the REs in the MEA for the study of the anode overpotentials; (d) transverse view of the channels, and (e) approximate distance between the REs along the channels. The numbering follows the hydrogen path, where RE 1 is close to the anode inlet, 2 is halfway along the anode path and 3 is at the anode outlet.

distinctive phases. $\Delta\eta$ was calculated by subtracting the anode potential measured during operation with pure H_2 from that in the presence of CO in order to quantify directly the effect of CO at each location. The transition phase comprises the time from the introduction of CO until a pseudo-steady state is reached. During both the transition phases and the pseudo-steady states, complex self-sustained potential oscillations are observed. Although oscillations are present, the average cell voltage and the CO_2 concentration remain almost constant during the pseudo-steady states. Fig. 2 (b) presents the evolution of the CO_2 concentration measured at the anode outlet during the transition phases and at the pseudo-steady states. Finally, the recovery phase evaluates the behaviour of the system when the CO is removed and pure H_2 is reinstated. In the preliminary experiments presented in the Supplementary Information (S1), no self-sustained potential oscillations are observed due to the lower CO concentration, which is known to determine the appearance and variation of patterns in the observed anode potential and cell voltage [5]. However, a clear trend in the anode potential, related to the CO coverage, shows comparative benchmarks [25,26] which validate this experimental setup.

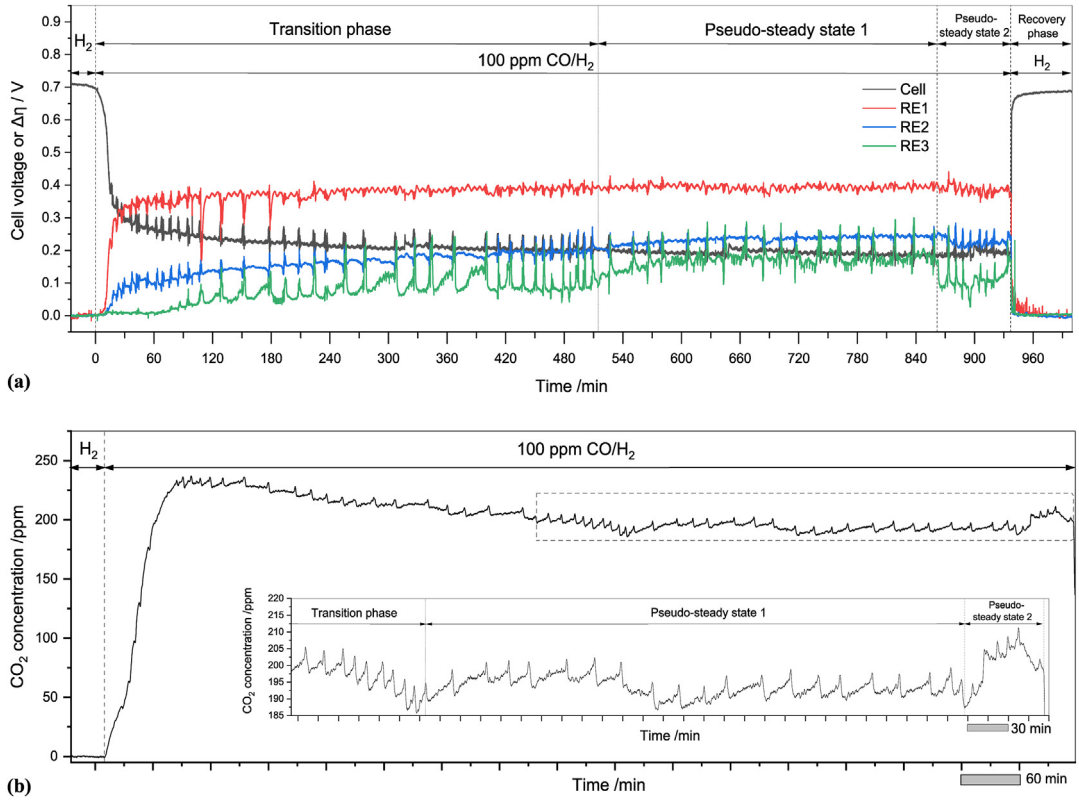

Fig. 2 – (a) Evolution of cell voltage and anode overpotential change due to CO ($\Delta\eta$) measured against the three REs in a PEMFC under galvanostatic control (0.3 A cm^{-2}) during the operation with pure H_2, followed by the operation with a mixture of 100 ppm CO/H_2 for ~16 h and a final stage with pure H_2. The transition phase, the pseudo-steady states, and the recovery phase under study are identified; and, (b) evolution of the CO_2 concentration during the transition phase and the pseudo-steady states. The RE numbering follows the hydrogen path through the flow-field, where RE1 is closest to the anode inlet.

Transition phase

The decrease in overall cell voltage observed in Fig. 2 (a) in the presence of CO is attributed to the evolving increase in anode overpotential, starting from the inlet and progressing along the anode flow-field. During the first minutes of exposure to CO, $\Delta\eta$ remains close to zero before an increase is eventually observed sequentially at all three RE locations. This time period is dependent on the mass transport of CO to the catalyst surface, the rate of CO adsorption and on the distance from the anode inlet, as the catalyst sites closer to the inlet are first exposed to CO. As such, the CO is being extracted from the feed stream. As these areas become saturated, less CO is available to poison downstream locations. This results in the observed increasing order of this 'induction' time at the three RE locations, where RE1 is the first to be affected at ~5 min, followed by RE2 at ~11 min and RE3 at ~61 min. The induction times are shown more clearly in Fig. 3 (a) where the evolution of the cell voltage and $\Delta\eta$ for the three REs are shown for the ~16 h of exposure to CO in a logarithmic plot.

In Fig. 3 (a), it is observed that the induction period is followed by an increase in $\Delta\eta$, confirming the poisoning of the catalyst which impedes the hydrogen oxidation reaction (HOR). Throughout this transition phase, the evolution of $\Delta\eta$ with time follows a characteristic S-shape (sigmoidal), which can be described using the logistic function which is commonly used to describe transition phenomena in various fields, including the kinetics of autocatalytic and biomolecular reactions [54], crystallization [55], wetting [56] and dewetting [57] processes. This model has also been used in conjunction with other machine learning methods to predict PEMFC performance [58]. To the authors' knowledge, the logistic function has not been used to analyse experimental PEMFC data. Through this function, it is possible to estimate the time needed to advance from 10% to 90% of the first pseudo-steady state value of $\Delta\eta$ for the different RE locations [65], as detailed in the Supporting Information (S2). The approximate transition times are shown in Fig. 3 (b) and confirm the more rapid poisoning closer to the anode inlet, with the rate decreasing towards the outlet. At RE1, the approximate transition time was 22 min, while for RE2 and RE3 it was 51 min and 488 min, respectively. The transition time for the entire cell to reach the pseudo-steady state is consequently higher than 488 min. Bender et al. presented a different methodology for the determination of the transition time in cases where the cells are contaminated by low concentrations of CO (1–2 ppm CO/H_2); no self-sustained oscillations were observed and a linear fit of $\Delta\eta$ versus time was possible [45]. In the present study, the concentration of CO_2 in the anode outlet was also taken into consideration for the depiction of the transition phase. In Fig. 2 (b) an increase in the CO_2 concentration due to the

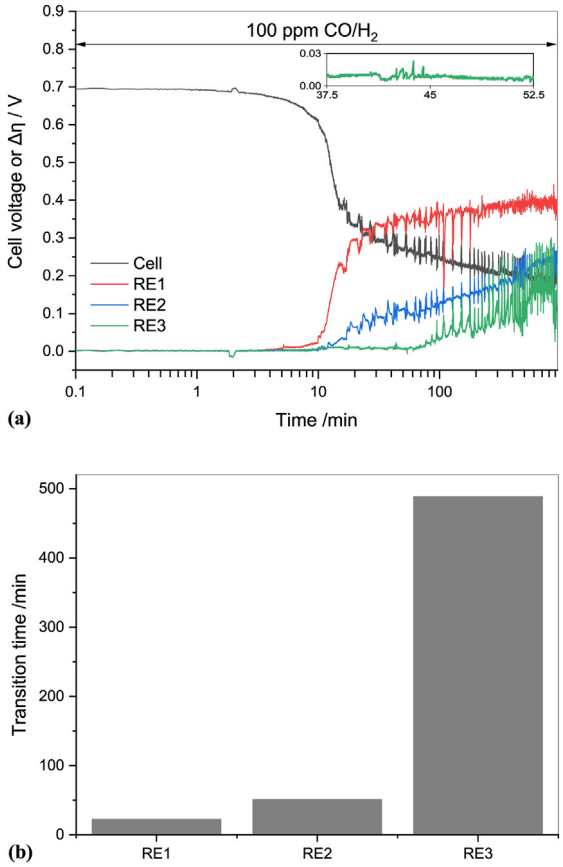

Fig. 3 – (a) Evolution of cell voltage and anode overpotential change due to CO ($\Delta\eta$) measured against the three REs in a PEMFC exposed to 100 ppm CO/H_2 under galvanostatic control (0.3 A cm^{-2}) during operation with CO/H_2 for 16 h (logarithmic plot). The inset presents $\Delta\eta$ at RE3 during the induction period, where self-sustained potential oscillations are observed. (b) Estimated transition time to go from 10% to 90% of the pseudo-steady state $\Delta\eta$, obtained through a logistic model. The RE numbering follows the hydrogen path through the flow-field, where RE1 is closest to the anode inlet.

oxidation of CO entering the cell is observed. During the first hours of exposure, CO is rapidly adsorbed into the catalyst sites, while CO oxidation occurs slowly at low potentials [59]. The CO oxidation rate increases as the electrode potential rises. A constant average concentration is reached at ~515 min (8.6 h) from the injection of CO to the system, which is indicative of the equilibrium between the CO adsorption and oxidation in the cell.

The more rapid contamination closer to the anode inlet is due to the progressive adsorption of CO along the flow-field path, leading to a longer induction time with increasing channel distance. The area closer to the anode inlet adsorbs and partially oxidises CO from the gas stream, reducing the CO concentration downstream. As a result, the rate of increase of $\Delta\eta$ following the induction period decreases towards the end of the channel, delaying the transition to a pseudo-steady state. As such, areas of the catalyst upstream are extracting CO from the feed by adsorption and oxidation to CO_2, effectively 'purifying' the stream to the advantage of downstream catalyst sites.

Other aspects to take into consideration to explain the progressive increase of the transition time towards the anode outlet are the local operating conditions throughout the cell. The effects of local humidity are of particular interest, as the CO stripping potential of Pt/C decreases with increasing water vapour pressure [19], and condensation of water in the catalyst layer pores leads to a decrease in the CO diffusion rate to the Pt surface [60]. According to in situ measurements of relative humidity in a similar cell operating with pure H_2, the relative humidity in the anode gas channel increases from inlet to outlet due to back-diffusion of water from the cathode [61]. Moreover, the poisoning of the electrode surface leads to inhomogeneous current density distribution. Studies have shown that for a constant overall cell current, the anode inlet tends to present a lower current density due to localised poisoning, while the current density increases towards the outlet to ensure the same overall current is generated by the cell [25,26]. The production of water closer to the anode outlet is consequently intensified, contributing to enhanced oxidation of CO in this region.

In this transition phase, complex self-sustained potential oscillations emerge across the active area of the cell. The $\Delta\eta$ oscillations are observed at all three RE locations, including RE3, where very small oscillations are present in the induction phase, and the major effects of the poisoning have not occurred in the first 61 min of exposure to CO. As the CO concentration builds up in the area of RE3, the amplitude of the oscillations gradually increases until the pseudo-steady state is reached, as observed in Fig. 3 (a).

The appearance of the oscillations in all three RE locations, despite the variation of the CO concentration and humidity, is explained by the electrical coupling throughout the cell, as described by the models presented by Hanke-Rauschenbach and co-workers [31,32,40]. It is inferred that the process starts with the adsorption of CO in the area closer to the anode inlet, which is more severely poisoned due to its proximity to the entrance. This area reaches the overpotential threshold for the occurrence of CO oxidation and the consequent self-sustained potential oscillations ensue. Due to mean-field and migration coupling interactions, oscillations are observed throughout the cell, even if the local anode overpotential is lower towards the anode outlet (RE3) and during the induction phase where the CO content is low. The complex pattern observed is examined in detail in the next section.

Pseudo-steady states

Two pseudo-steady states were identified in this experiment, where the delimitation is mainly marked by a change in the frequency of the self-sustained oscillations observed, from a period of ~19.5 min in pseudo-steady state 1, to ~9.5 min in pseudo-steady state 2. These periods are considerably longer than reported in previous studies due to the larger cell, lower flow rate, higher temperature and the use of pure Pt in this work. In Fig. 4 (a), the average cell voltage, $\Delta\eta$ at different RE locations and CO_2 concentration at the anode outlet at these two states are presented. Measurements taken between 515

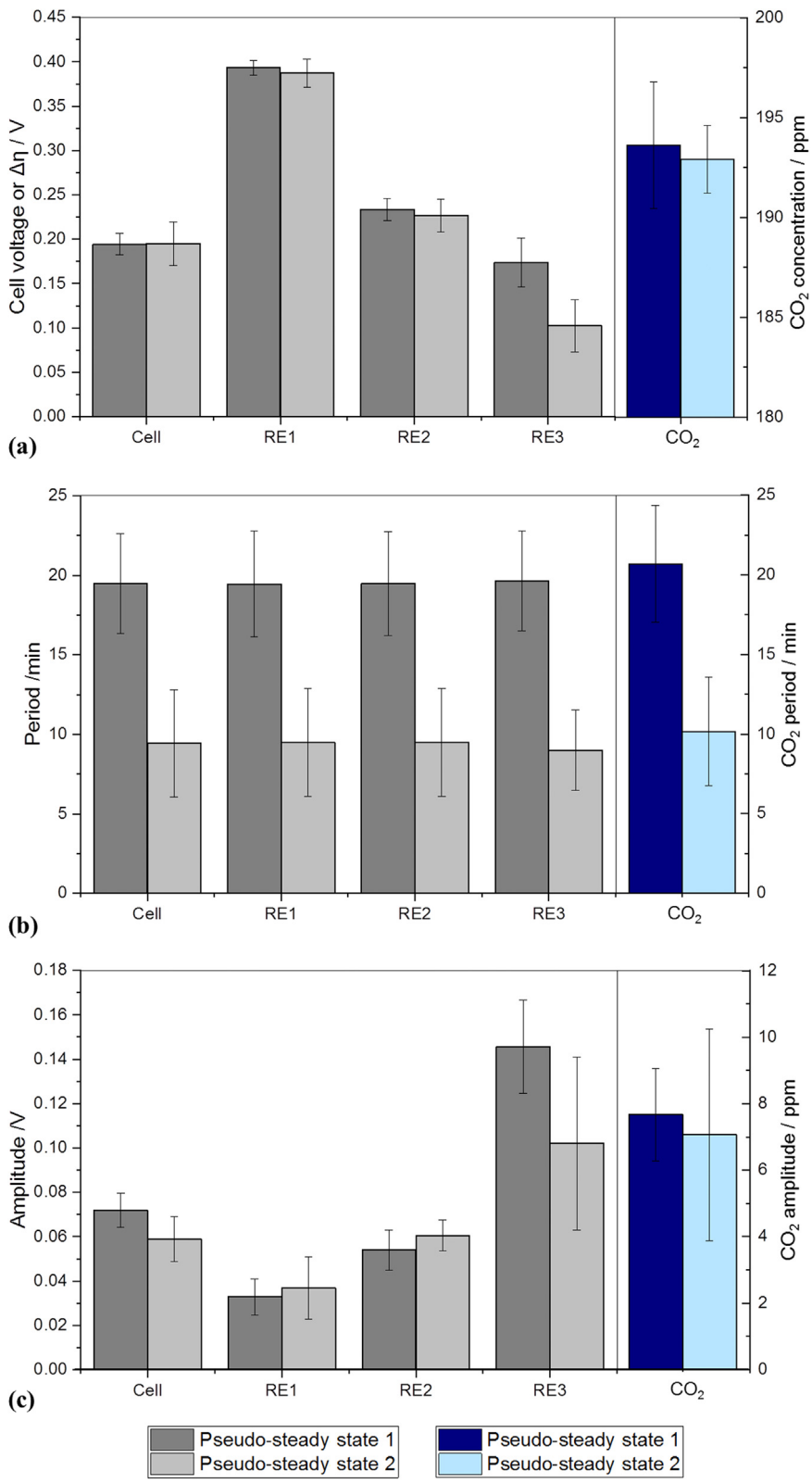

Fig. 4 – Depiction of the pseudo-steady states observed in a 50 cm^2 PEMFC exposed to 100 ppm CO/H_2 and controlled galvanostatically at 0.3 A cm^{-2}. Pseudo-steady state 1 covers the period between ~515 and ~863 min, and the pseudo-steady state 2 starts at ~863 and finishes at ~937 min after the introduction of CO. (a) Average cell voltage, anode overpotential change $\Delta\eta$ at the different locations of the REs, and CO_2 concentration at the anode outlet; and, (b) period and (c) peak-to-peak amplitude of the self-sustained potential oscillations observed. The RE numbering follows the hydrogen path, where RE1 is closest to the anode inlet.

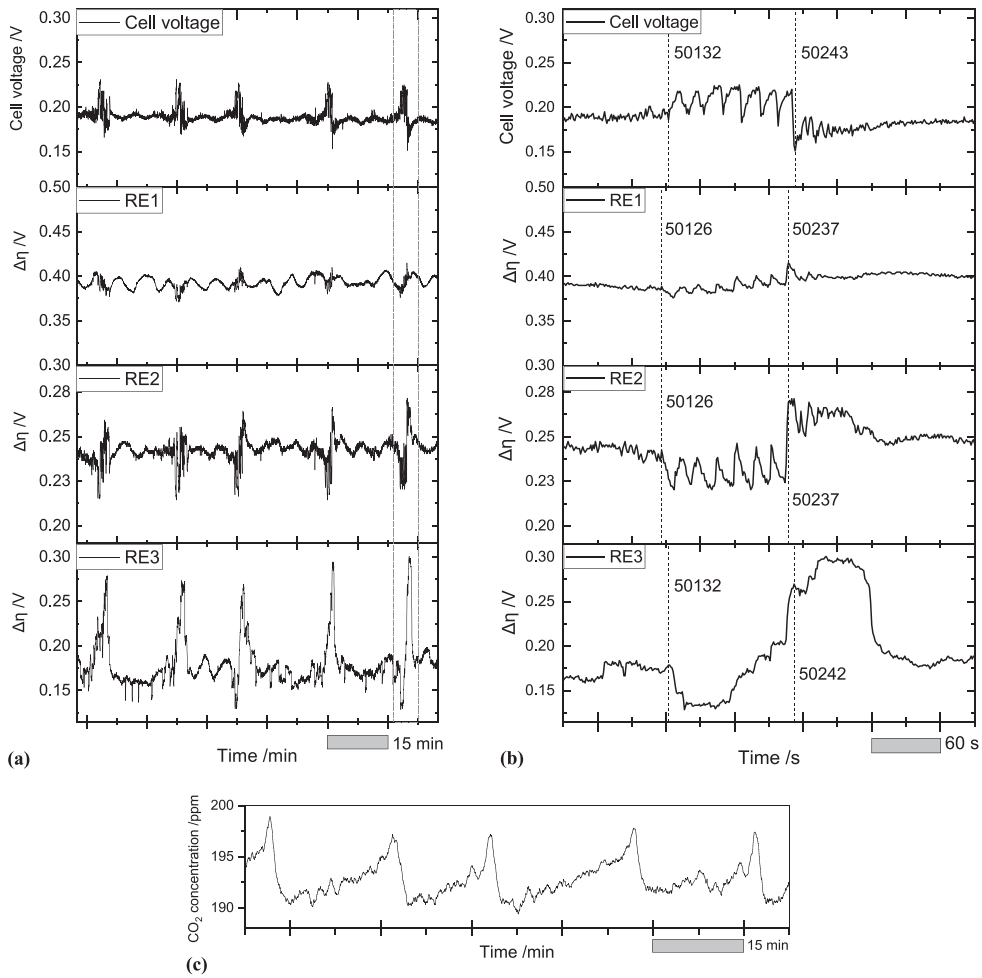

Fig. 5 – Self-sustained oscillations of the cell voltage and the anode overpotential change ($\Delta\eta$) in the pseudo-steady state 1, measured against the three localised REs in a PEMFC exposed to 100 ppm CO/H_2 under galvanostatic control (0.3 A cm^{-2}), in the space of (a) 1.5 h after ~12.5 h of exposure, (b) 6 min after ~14 h of exposure. (c) CO_2 concentration oscillations in the space of 1.5 h in the pseudo-steady state 1. The RE numbering follows the hydrogen path, where RE1 is closest to the anode inlet.

and 863 min after the introduction of CO were considered part of the pseudo-steady state 1, while the range between 863 and 937 min (before the reintroduction of H_2) covers the pseudo-steady state 2. In the course of both states, the overall cell has a very low voltage indicative of almost complete deactivation of performance. It is confirmed that the average $\Delta\eta$ varies significantly across the active area of the cell. The area closer to the anode inlet is more affected due to exposure to a higher concentration of CO and lower relative humidity. As the concentration of CO decreases along the channel and the relative humidity increases towards the anode outlet, at RE2 the $\Delta\eta$ measured is lower than at RE1, but higher than at RE3. The area towards the exit of the cell is much less poisoned by the CO entering the cell, even after a prolonged period of time.

Fig. 5 (a) presents the evolution of cell voltage and $\Delta\eta$ over a period of 1.5 h at the three RE locations following ~12.5 h of CO exposure, during which a sequence of oscillations is observed at all three locations in the pseudo-steady state 1 region. The complex behaviour of the cell voltage during the oscillation period is confirmed, whereby mixed mode oscillations (MMOs), composed of large and small amplitude oscillations, are observed [62]. In this case a cascade of up to seven small oscillations is observed per each large oscillation (Fig. 5 (b)). Similar behaviour was observed at low flow rates and high current densities by Mota et al. who correlated the different maxima to a series of oxidation steps [12]. Following the model presented by Hanke-Rauschenbach et al., it could also be inferred that the complex pattern of the oscillations is related to the flow rate regime, where the time constant for CO transport in the channel (or cell in this case) is longer than that for the adsorption of CO. The cycle starts with the partial coverage of the active area by CO, the anode potential increases and prompts a first oxidation step in this part of the cell. The remaining CO continues to be adsorbed on the rest of

the catalyst surface, leading to multiple oxidation peaks [31]. A simplification of this model, presented by Kirsch et al., provides further insight into the dominant interactions occurring throughout the cell, as the pattern observed is associated with dominant mean-field coupling in combination with a low flow rate [32,40].

The simultaneous measurement of the overall cell voltage and local $\Delta\eta$ profiles allows for the evaluation of spatio-temporal dynamics of the oscillation process. A detailed view of one oscillation period over 6 min towards the end of this period is presented in Fig. 5 (b). It is shown that the evolution of $\Delta\eta$ for RE1 and RE2 is in the opposite direction to the cell voltage as expected. A rise in the CO oxidation rate leads to a decrease in the CO coverage, reducing $\Delta\eta$ and increasing the cell voltage. Similarly, cell voltage drops with increase in CO adsorption, which hampers H_2 oxidation rate. The sequence of the period-doubling bifurcation is well defined at these two locations. However, at RE3 the evolution of $\Delta\eta$ differs from that at RE1 and RE2, as a lower number of bifurcation periods is observed. In some cases, $\Delta\eta$ at RE3 decreases while an increase is observed at RE1 and RE2, and vice versa. There is no defined trend in the increase of $\Delta\eta$ to the highest peak of the oscillation in RE3. This behaviour suggests defect turbulence in this area. Moreover, the oscillations are not in phase across the active area of the cell. Two points at the start and the end of the period-doubling bifurcation series were chosen to elucidate the sequence of events. These are indicated by the dotted lines in Fig. 5 (b) and include the time in seconds from the introduction of CO to the cell. It is observed that while the $\Delta\eta$ variations are simultaneous in RE1 and RE2, there is a delay of 5–6 s in RE3 demonstrating phase turbulence. The oscillations in the cell voltage reflect the anode overpotential of the overall cell and occur between RE1/RE2 and RE3.

While the evolution of the overall cell voltage implies a global dominant mean-field coupling in conjunction with a low flow rate (a stoichiometry of 2, which is more representative of real operating conditions) due to the defined series of bifurcation periods, the study of local $\Delta\eta$ variations reveals that both mechanisms can coexist across different cell locations. The well-defined $\Delta\eta$ profiles at RE1 and RE2 imply that the dominant interaction between the individual oscillators is mean-field coupled in the area near the anode inlet (RE1) and centre (RE2). However, the differences observed at RE3 indicate phase and defect turbulence, characteristic of migration coupling. As a larger area of the cell is dominated by mean-field coupling, this behaviour is reflected in the overall cell voltage profile. This result provides experimental support for the model presented by Kirsch et al., where the coexistence of a dominant mean-field coupling inlet area and a dominant migration coupling outlet region was predicted in a straight channel. The membrane conductivity and the system dimensions were identified as determinative for the relative dominance of these interactions [32].

As for the electrochemical turbulence occurring in the outlet region of the anode, previous studies have presented evidence of phase and defect turbulence in a PEMFC exposed to CO under potentiostatic control [40], although to our knowledge this behaviour has not been reported experimentally under galvanostatic control. Considering the dominant migration coupling, this area is more influenced by the local operating conditions where the CO coverage is limited and the relative humidity is higher. It is inferred that these conditions contribute to the reduction of the number of the oxidation steps that compose the cascade or doubling bifurcation periods. It is also important to mention that the model was originally proposed for a single channel and not the six-channel serpentine flow-field used in this work, which is more technologically relevant. Previous studies indicated that an increase in the membrane resistance could lead to a transition from a mean-field coupling to a chaotic regime [32,40]. However, in this work, a lower membrane resistance is inferred in the area closer to the anode outlet, where the electrochemical turbulence is observed, compared to the rest of the cell. This highlights an important limitation in the model which assumes a constant conductivity in space and time. Further studies are required to elucidate the influence of membrane resistance on the dominant coupling mechanism.

The variation in the CO oxidation rate during the self-sustained oscillations is reflected in the variation of the CO_2 concentration at the anode outlet as shown in Fig. 5 (c), where oscillations are also observed. In each cycle, the concentration of CO_2 increases as a result of the oxidation of CO in the cell. Several spikes are observed, confirming the multiple oxidation steps related to the distribution of oscillatory behaviour across the cell as seen in Fig. 5 (a) and (b).

The periodicity of the oscillations observed in the evolution of the cell voltage, the $\Delta\eta$ at the three RE locations and the concentration of CO_2 in the anode outlet was measured at the two pseudo-steady states. Even though there is a difference in the starting points of the oscillations in the $\Delta\eta$ throughout the cell and the cell voltage, each cycle occurs every ~19.5 min for each one of the parameters studied in the pseudo-steady state 1, as shown in Fig. 4 (b). The matched frequencies are related to the mean-field coupling across the cell. Even though the region closer to the anode outlet is dominated by the migration coupling, the impact of the mean-field coupling is not negligible and influences the duration of each period. This is consistent with the simulation work by Kirsch et al. that evaluated the impact of mean-field and migration coupling in the formation of patterns. In the case of a more realistic situation, where both interactions are present, the synchronisation of the frequencies occurred at high membrane conductivities values (~1 S m^{-1}). It was proposed that at high membrane conductivities, mean-field coupling tends to dominate migration coupling [32], reinforcing the importance of studying the impact of membrane conductivity in the competition between the two interactions. In the case of the pseudo-steady state 2, the period is ~9.5 min for the parameters mentioned. The increase in the oscillation frequency is associated with the variation in local operating conditions, such as liquid water accumulation or an alteration of the catalyst layer, probably closer to the anode outlet, where the changes in the $\Delta\eta$, the period and the amplitude of the oscillations are more pronounced (Fig. 4). Due to the overall dominance of the mean-field coupling, the alterations in a small area are reflected in the rest of the cell.

The comparison of the average peak-to-peak amplitude (*i.e.*, the difference between the minimum and maximum) of the oscillations in the cell voltage and the $\Delta\eta$ at the three RE locations at the two pseudo-steady states is presented in Fig. 4 (c), where increasing peak-to-peak amplitude of the $\Delta\eta$ towards the area closer to the anode outlet is observed. This variation is a result of the previously mentioned redistribution of the current density in the presence of CO under galvanostatic control. Kadyk et al. related an increasing current to an increase in the amplitude of the self-sustained potential oscillations [10]; therefore, lower amplitudes in the area closer to the anode inlet are expected where a decrease in current is presented, with higher amplitudes closer to the outlet where an increase in the current density is sustained.

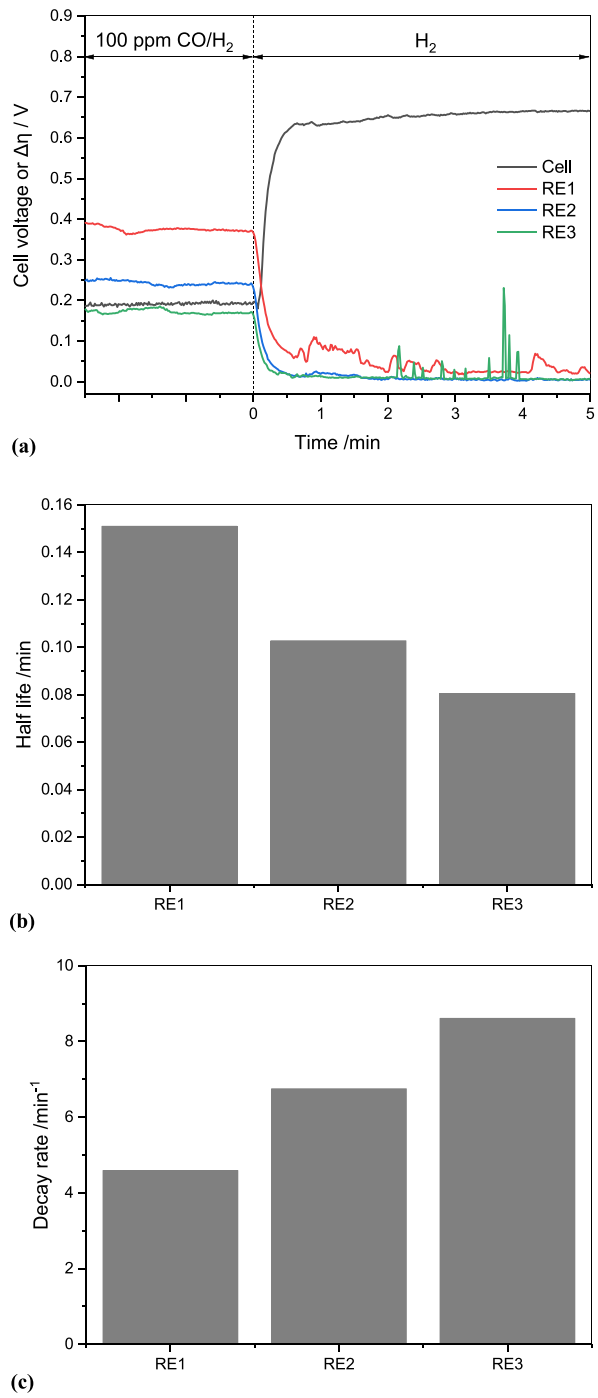

Fig. 6 – Recovery of a PEMFC exposed to 100 ppm CO/H_2 at constant current (0.3 A cm^{-2}) by the reintroduction of H_2. (a) Exponential decay of the anode overpotential change ($\Delta\eta$) at the three RE locations and the corresponding increase of the cell voltage; (b) half-life and, (c) decay rate of the anode overpotential change $\Delta\eta$ measured at the three RE locations as calculated from the exponential decay model.

Finally, another trend in this phase is observed in Fig. 3 (a), where the average $\Delta\eta$ at each RE location presents a gradual increase over time. This variation is presumably due to catalyst degradation, as previous studies have demonstrated an increased loss of electrochemical surface area in the short and long term in the presence of CO [52]. No previous studies have evaluated the effects of self-sustained potential oscillations on catalyst degradation; and in particular the spatially-resolved deterioration of the catalyst in the long term. In this relatively short experiment, it is possible to observe a higher increase in the average $\Delta\eta$ closer to the anode outlet (RE3). Considering the differences in the amplitude of the oscillations studied in Fig. 4 (c), it is deduced that the greater fluctuations in $\Delta\eta$ indicate an increase in the loss of catalyst surface area. As the amplitude of the oscillations increases towards the anode outlet, the catalyst degradation is also intensified towards the anode outlet. The ageing effect of CO-induced potential oscillations on catalyst materials requires further study.

Recovery phase

Fig. 6 (a) shows how the cell responds when the CO is removed from the hydrogen feed. An immediate decrease in $\Delta\eta$ is observed at all three RE locations upon introduction of pure hydrogen, which leads to an increase in cell voltage that plateaus in less than 1 min. Compared to the initial phase of poisoning, the recovery is a much faster process at all RE locations. It should be noted that the initial recovery of the cell is not due to the complete removal of the CO from the catalyst surface, but because sufficient CO has been removed that H_2 activation is no longer the rate-limiting step [63].

The kinetics of the CO displacement by H_2 in Pt(111) surfaces has been identified as a first-order process [64], and considering the direct impact of the CO coverage on $\Delta\eta$, an exponential model was used to compare the time required to reach steady anode overpotential. The time at the introduction of pure H_2 was set to 0, and an exponential model described in the Supporting Information (S3) was utilised. Fig. 6 (b) and (c) present the half-life and decay rate (recovery rate) at each of the RE locations. It is observed that the half-life decreases towards the anode outlet due to lower CO coverage at pseudo-steady state. The time required for CO removal is longer towards the inlet mainly due to higher CO surface coverage, as expected. In terms of the recovery rate, a homogeneous active area and operating conditions across the electrode would have implied a constant rate; however, it increases towards the outlet demonstrating the influence of parameters other than CO coverage on the reaction rate. As in the transition phase and pseudo-steady states, it is assumed that the local operating conditions play a significant role in cell recovery. For instance, CO oxidation is enhanced in the vicinity of the anode inlet (RE1) due to higher anode overpotential, whereas higher local relative humidity prompt enhanced CO oxidation near the anode outlet (RE3). The faster recovery closer to the anode outlet is also due to the higher humidity, as the strong bond between the H_2O molecules and the Pt facilitates faster CO desorption [60]. These parameters vary over time as the cell recovers, and their evolution and influence in this process are important subjects study for the development and optimisation of mitigation strategies against CO poisoning.

Conclusions

Localised reference electrodes were used to measure the change in the anode overpotential of a cell exposed to 100 ppm CO/H_2 on the anode under galvanostatic control. The location of the reference electrodes over the MEA provided information on the distribution and dynamics of the poisoning process. The poisoning process, as indicated by the anode overpotential, follows a sigmoidal function with time. This is notionally split into three phases, an initial slow induction period, a rapid transition period and two pseudo-steady state periods. It was observed that the sites near the anode inlet reached the pseudo-steady state faster and presented a higher $\Delta\eta$ than the sites closer to the outlet due to the exposure to a higher CO concentration and lower relative humidity.

Mixed-mode oscillations were observed in the cell voltage and the anode overpotential across the electrode during the transition phase and at the pseudo-steady state. In agreement with the model and the subsequent simplifications presented by Hanke-Rauschenbach et al., the system was analysed as a series of individual oscillators [31,32,40]. The coexistence of a dominant mean-field coupling area at the anode inlet and centre, and a dominant migration coupling region closer to the anode outlet was demonstrated. The dominant mean-field coupling area was characterised by defined and simultaneous oscillations in the $\Delta\eta$ profiles, while phase and defect turbulence were observed in the area where the migration coupling field was dominant. This result is in agreement with model predictions for a single straight channel by Kirsch et al. [32]. Moreover, electrochemical turbulence closer to the anode outlet was experimentally reported for the first time under galvanostatic control and under operating conditions closer to real-world applications. A second pseudo-steady state was identified, where the most important variation in the parameters studied was an increase in the frequency of the oscillations. More studies are needed in order to elucidate the shift between these two states, although it was presumed that a variation in the operating conditions in a small section of the cell (such as liquid water accumulation or alteration of the catalyst layer) was equally observed in the rest of the cell due to dominant mean-field coupling.

Additionally, a correlation between voltage oscillations and CO oxidation was demonstrated by measuring the CO_2 concentration at the anode outlet. The period of the oscillations was similar for the cell voltage, each one of the $\Delta\eta$ profiles throughout the cell and the CO_2 concentration at the anode outlet due to the dominant mean-field coupling across the cell, despite the presence of the migration interaction closer to the anode outlet. Future studies should evaluate the transition from a mean-field coupling dominance to a migration coupling one. The amplitude of the oscillations was nonetheless found to increase towards the anode outlet, as a result of heterogeneous current density distribution (being larger towards the anode outlet) and the varying CO coverage and relative humidity.

Cell recovery upon reintroduction of pure H_2 has been shown to be a more rapid process than the poisoning phase. An exponential fit was used to compare local recovery rates, which were found to be closely related to the CO coverage; the area near the anode inlet (RE1) demonstrated a slower decay rate and a higher half-life due to higher CO coverage. Other parameters to take into account are the relative humidity and anode overpotential, which affect the CO oxidation rate and vary across the electrode during this phase.

Finally, the study of the poisoning dynamics across the active area of the cell during the different phases of the poisoning provides valuable information for the design and optimisation of more efficient CO poisoning mitigation strategies. For instance, an area with a more active catalyst that enhances the oxidation of CO could be considered closer to the anode inlet where the contamination is more severe.

Declaration of competing interest

The authors declare that they have no known competing financial interests or personal relationships that could have appeared to influence the work reported in this paper.

Acknowledgements

VFVL acknowledges the Mexican National Council of Science and Technology (CONACYT) for the financial support (405938). The authors would like to acknowledge funding from the EPSRC (EP/L015277/1, EP/P009050/1, EP/M014371/1, EP/M009394/1, EP/M023508/1, EP/L015749/1, EP/N022971/1) for supporting fuel cell research in the Electrochemical Innovation Lab (EIL). This work was supported by the National Measurement System of the UK Department of Business, Energy & Industrial Strategy. PRS and DJLB acknowledge the Royal Academy of Engineering for support of their respective Research Chairs.

Appendix A. Supplementary data

Supplementary data to this article can be found online at https://doi.org/10.1016/j.ijhydene.2022.10.007.

REFERENCES

[1] USDOE. Fuel Cells, http://energy.gov/eere/fuelcells/fuel-cells. [Accessed 10 August 2020].
[2] Cheng X, Shi Z, Glass N, Zhang L, Zhang J, Song D, et al. A review of PEM hydrogen fuel cell contamination: impacts, mechanisms, and mitigation. J Power Sources 2007;165:739–56.
[3] Oetjen HF, Schmidt VM, Stimming U, Trila F. Performance data of a proton exchange membrane fuel cell using H2/CO as fuel gas. J Electrochem Soc 1996;143:3838–42.
[4] Murthy M, Esayian M, Hobson A, MacKenzie S, Lee WK, Van Zee JW. Performance of a polymer electrolyte membrane fuel cell exposed to transient CO concentrations. J Electrochem Soc 2001;148:A1141–7.
[5] Zhang J, Datta R. Sustained potential oscillations in proton exchange membrane fuel cells with PtRu as anode catalyst. J Electrochem Soc 2002;149:A1423–31.
[6] Zhang J, Fehribach JD, Datta R. Mechanistic and bifurcation analysis of anode potential oscillations in PEMFCs with CO in anode feed. J Electrochem Soc 2004;151:A689–97.
[7] Deibert MC, Williams DL. Voltage oscillations of the H2-CO system. J Electrochem Soc 1969;116:1290.
[8] Lopes PP, Ticianelli EA, Varela H. Potential oscillations in a proton exchange membrane fuel cell with a Pd–Pt/C anode. J Power Sources 2011;196:84–9.
[9] Nogueira JA, Varela, H. Voltage oscillations in a polymer electrolyte membrane fuel cell with Pd-Pt/C and Pd/C anodes. ChemistryOpen;6:629-636.
[10] Kadyk T, Kirsch S, Hanke-Rauschenbach R, Sundmacher K. Autonomous potential oscillations at the Pt anode of a polymer electrolyte membrane fuel cell under CO poisoning. Electrochim Acta 2011;56:10593–602.
[11] Lu H, Rihko-Struckmann L, Hanke-Rauschenbach R, Sundmacher K. Spontaneous oscillations of cell voltage, power density, and anode exit CO concentration in a PEM fuel cell. Phys Chem Chem Phys 2011;13:18179–85.
[12] Mota A, Lopes PP, Ticianelli EA, Gonzalez ER, Varela H. Complex oscillatory response of a PEM fuel cell fed with H2/CO and oxygen. J Electrochem Soc 2010;157:B1301–4.
[13] Heuer M, Bernstein PA, Wenske M, Styczynski ZA. Results of current density distribution mapping in PEM fuel cells dependent on operation parameters. Energies 2013;6:3841–58.
[14] Pei H, Liu Z, Zhang H, Yu Y, Tu Z, Wan Z, et al. In situ measurement of temperature distribution in proton exchange membrane fuel cell I a hydrogen–air stack. J Power Sources 2013;227:72–9.
[15] Schneider IA, Kramer D, Wokaun A, Scherer GG. Spatially resolved characterization of PEFCs using simultaneously neutron radiography and locally resolved impedance spectroscopy. Electrochem Commun 2005;7:1393–7.
[16] Schneider IA, Kuhn H, Wokaun A, Scherer GG. Study of water balance in a polymer electrolyte fuel cell by locally resolved impedance spectroscopy. J Electrochem Soc 2005;152:A2383.
[17] Kalyvas C, Kucernak A, Brett D, Hinds G, Atkins S, Brandon N. Spatially resolved diagnostic methods for polymer electrolyte fuel cells: a review. Wiley Interdiscip Rev: Energy Environ 2014;3:254–75.
[18] Dhar HP, Christner LG, Kush AK. Nature of CO adsorption during H 2 oxidation in relation to modeling for CO poisoning of a fuel cell anode. J Electrochem Soc 1987;134:3021–6.
[19] Ioroi T, Yasuda K, Miyazaki Y. Humidity dependence of the oxidation of carbon monoxide adsorbed on Pt/C and PtRu/C electrocatalysts. Phys Chem Chem Phys 2002;4:2337–40.
[20] Zhou F, Andreasen SJ, Kær SK, Park JO. Experimental investigation of carbon monoxide poisoning effect on a PBI/H3PO4 high temperature polymer electrolyte membrane fuel cell: influence of anode humidification and carbon dioxide. Int J Hydrogen Energy 2015;40:14932–41.
[21] Jiang R, Kunz HR, Fenton JM. Electrochemical oxidation of H2 and H2 / CO mixtures in higher temperature (T cell 100 ° C) proton exchange membrane fuel cells: electrochemical impedance spectroscopy. J Electrochem Soc 2005;152:A1329–40.
[22] Díaz MA, Iranzo A, Rosa F, Isorna F, López E, Bolivar JP. Effect of carbon dioxide on the contamination of low temperature and high temperature PEM (polymer electrolyte membrane) fuel cells. Influence of temperature, relative humidity and analysis of regeneration processes. Energy 2015;90:299–309.
[23] Zhang J, Thampan T, Datta R. Influence of anode flow rate and cathode oxygen pressure on CO poisoning of proton exchange membrane fuel cells. J Electrochem Soc 2002;149:A765–72.

[24] Murthy M, Esayian M, Lee WK, Van Zee JW. The effect of temperature and pressure on the performance of a PEMFC exposed to transient CO concentrations. J Electrochem Soc 2003;150:A29–34.
[25] Reshetenko TV, Bethune K, Rocheleau R. Spatial proton exchange membrane fuel cell performance under carbon monoxide poisoning at a low concentration using a segmented cell system. J Power Sources 2012;218:412–23.
[26] Reshetenko TV, Bethune K, Rubio MA, Rocheleau R. Study of low concentration CO poisoning of Pt anode in a proton exchange membrane fuel cell using spatial electrochemical impedance spectroscopy. J Power Sources 2014;269:344–62.
[27] Murahashi T, Mitsumoto T, Nishiyama E. Current distribution of a PEMFC under CO poisoning. ECS Trans 2009;25:869–79.
[28] Boaventura M, Sander H, Friedrich KA, Mendes A. The influence of CO on the current density distribution of high temperature polymer electrolyte membrane fuel cells. Electrochim Acta 2011;56:9467–75.
[29] Bender G, Zawodzinski TA. Spatial distribution of the CO transient response of a PEFC. 3rd symposium on proton conducting membrane fuel cells. Salt Lake City, UT: Electrochemical Society, Inc.; 2002. p. 212–9.
[30] Gardner CL, Mehta D, Chugh S, Kjeang E. Modeling the spatial and temporal distribution of current in a carbon monoxide poisoned polymer electrolyte fuel cell using a dynamic pseudo 1-D approach. J Electrochem Soc 2019;166:F3123–35.
[31] Hanke-Rauschenbach R, Kirsch S, Kelling R, Weinzierl C, Sundmacher K. Oscillations and pattern formation in a PEM fuel cell with Pt/Ru anode exposed to H2/CO mixtures. J Electrochem Soc 2010;157:B1521–8.
[32] Kirsch S, Hanke-Rauschenbach R, Sundmacher K. Analysis of spatio-temporal pattern formation in a PEM fuel cell with Pt / Ru anode exposed to H2 / CO mixtures. J Electrochem Soc 2011;158:B44–53.
[33] Eiswirth M, Möller P, Wetzl K, Imbihl R, Ertl G. Mechanisms of spatial self-organization in isothermal kinetic oscillations during the catalytic CO oxidation on Pt single crystal surfaces. J Chem Phys 1989;90:510–21.
[34] Falcke M, Engel H. Influence of global coupling through the gas phase on the dynamics of CO oxidation on Pt(110). Phys Rev E 1994;50:1353–9.
[35] Mazouz N, Flätgen G, Krischer K. Tuning the range of spatial coupling in electrochemical systems: from local via nonlocal to global coupling. Phys Rev E 1997;55:2260–6.
[36] Brett DJL, Atkins S, Brandon NP, Vesovic V, Vasileiadis N, Kucernak AR. Investigation of reactant transport within a polymer electrolyte fuel cell using localised CO stripping voltammetry and adsorption transients. J Power Sources 2004;133:205–13.
[37] Benjamin TB, Hasselmann K, Lighthill MJ. Instability of periodic wavetrains in nonlinear dispersive systems. Proc Math Phys Eng Sci 1967;299:59–76.
[38] Varela H, Beta C, Bonnefont A, Krischer K. Transitions to electrochemical turbulence. Phys Rev Lett 2005;94:174104.
[39] Van-Gorder RA. Turing and Benjamin-Feir instability mechanisms in non-autonomous systems. Proc Math Phys Eng Sci 2020;476:20200003.
[40] Kirsch S, Hanke-Rauschenbach R, Stein B, Kraume R, Sundmacher K. The electro-oxidation of H2, CO in a model PEM fuel cell: oscillations, chaos, pulses. J Electrochem Soc 2013;160:F436–46.
[41] Valdés-López VF, Mason T, Shearing PR, Brett DJL. Carbon monoxide poisoning and mitigation strategies for polymer electrolyte membrane fuel cells – a review. Prog Energy Combust Sci 2020;79:100842.
[42] Wagner N, Gülzow E. Change of electrochemical impedance spectra (EIS) with time during CO-poisoning of the Pt-anode in a membrane fuel cell. J Power Sources 2004;127:341–7.
[43] Qi Z, He C, Kaufman A. Poisoning of proton exchange membrane fuel cell cathode by CO in the anode fuel. Electrochem Solid State Lett 2001;4:A204–5.
[44] Qi Z, He C, Kaufman A. Effect of CO in the anode fuel on the performance of PEM fuel cell cathode. J Power Sources 2002;111:239–47.
[45] Bender G, Angelo M, Bethune K, Rocheleau R. Quantitative analysis of the performance impact of low-level carbon monoxide exposure in proton exchange membrane fuel cells. J Power Sources 2013;228:159–69.
[46] Hinds G, Brightman E. In situ mapping of electrode potential in a PEM fuel cell. Electrochem Commun 2012;17:26–9.
[47] Lu H, Rihko-Struckmann L, Hanke-Rauschenbach R, Sundmacher K. Dynamic behavior of a PEM fuel cell during electrochemical CO oxidation on a PtRu anode. Top Catal 2008;51:89–97.
[48] Mota A, Gonzalez Ernesto R, Eiswirth M. Kinetic insights over a PEMFC operating on stationary and oscillatory states. J Phys Chem A 2011;115:13773–82.
[49] Lopes P, Batista B, Saglietti G, Varela H, Ticianelli E. Real-time determination of CO2 production and estimation of adsorbate coverage on a proton exchange membrane fuel cell under oscillatory operation. J Solid State Electrochem 2013;17:1851–9.
[50] Angelo M, Bender G, Dorn S, Bethune K, Hossain T, Posey D, et al. The impacts of repetitive carbon monoxide poisoning on performance and durability of a proton exchange membrane fuel cell. ECS Trans 2008;16:669–76.
[51] Franco AA, Guinard M, Barthe B, Lemaire O. Impact of carbon monoxide on PEFC catalyst carbon support degradation under current-cycled operating conditions. Electrochim Acta 2009;54:5267–79.
[52] Profatilova I, Jacques P-A, Escribano S. Evaluation of parameters accelerating the aging of PEMFCs operating under reformate containing carbon monoxide. J Electrochem Soc 2018;165:F3251–60.
[53] Chandesris M, Guetaz L, Schott P, Scohy M, Escribano S. Investigation of degradation heterogeneities in PEMFC stack aged under reformate coupling in situ diagnosis, post-mortem ex situ analyses and multi-physic simulations. J Electrochem Soc 2018;165:F3290–306.
[54] Reed LJ, Berkson J. The application of the logistic function to experimental data. J Phys Chem A 1928;33:760–79.
[55] Bian S, Du L-W, Gao Y-X, Huang J, Gou B-D, Li X, et al. Crystallization in aggregates of calcium phosphate nanocrystals: a logistic model for kinetics of fractal structure development. Cryst Growth Des 2012;12:3481–8.
[56] Taqvi ST, Almansoori A, Bassioni G. Modeling the impact of wettability alterations on calcium carbonate system for crude oil and asphaltenic solutions. Ind Eng Chem Res 2014;53:4773–7.
[57] Arscott S. Dynamic chemically driven dewetting, spreading, and self-running of sessile droplets on crystalline silicon. Langmuir 2016;32:12611–22.
[58] Legala A, Zhao J, Li X. Machine learning modeling for proton exchange membrane fuel cell performance. Energy and AI 2022;10:100183.
[59] Baschuk JJ, Li X. Carbon monoxide poisoning of proton exchange membrane fuel cells. Int J Energy Res 2001;25:695–713.
[60] Zhang JZ, Hongsirikarn K, Goodwin JG. The effect of low concentrations of CO on H2 adsorption and activation on Pt/C: Part 2—in the presence of H2O vapor. J Power Sources 2011;196:6186–95.

[61] Hinds G, Stevens M, Wilkinson J, de Podesta M, Bell S. Novel in situ measurements of relative humidity in a polymer electrolyte membrane fuel cell. J Power Sources 2009;186:52–7.
[62] Krischer K, Lübke M, Eiswirth M, Wolf W, Hudson JL, Ertl G. A hierarchy of transitions to mixed mode oscillations in an electrochemical system. Phys Nonlinear Phenom 1993;62:123–33.
[63] Zhang JZ, Liu Z, Goodwin JG. The effect of low concentrations of CO on H2 adsorption and activation on Pt/C. Part 1: in the absence of humidity. J Power Sources 2010;195:3060–8.
[64] Parker DH, Fischer DA, Colbert J, Koel BE, Gland JL. Hydrogen-induced CO displacement from the Pt(111) surface: an isothermal kinetic study. Surf Sci 1991;258:75–81.
[65] Panik MJ. Growth curve modeling: theory and applications. Hoboken, New Jersey: John Wiley & Sons, Inc.; 2014.